# REPORT DOCUMENTATION PAGE

*Form Approved*
*OMB No. 0704-0188*



| 1. REPORT DATE *(DD-MM-YYYY)* | 2. REPORT TYPE | 3. DATES COVERED *(From - To)* |
|---|---|---|
| | Technical Paper | |

**4. TITLE AND SUBTITLE**

**5a. CONTRACT NUMBER**

**5b. GRANT NUMBER**

**5c. PROGRAM ELEMENT NUMBER**

**6. AUTHOR(S)**

**5d. PROJECT NUMBER**

**5e. TASK NUMBER**

**5f. WORK UNIT NUMBER**

**7. PERFORMING ORGANIZATION NAME(S) AND ADDRESS(ES)**

**8. PERFORMING ORGANIZATION REPORT**

**9. SPONSORING / MONITORING AGENCY NAME(S) AND ADDRESS(ES)**

Air Force Research Laboratory (AFMC)
AFRL/PRS
5 Pollux Drive
Edwards AFB CA 93524-7048

**10. SPONSOR/MONITOR'S ACRONYM(S)**

**11. SPONSOR/MONITOR'S NUMBER(S)**

**12. DISTRIBUTION / AVAILABILITY STATEMENT**

Approved for public release; distribution unlimited.

**13. SUPPLEMENTARY NOTES**

**14. ABSTRACT**



**15. SUBJECT TERMS**

| 16. SECURITY CLASSIFICATION OF: | | | 17. LIMITATION OF ABSTRACT | 18. NUMBER OF PAGES | 19a. NAME OF RESPONSIBLE PERSON |
|---|---|---|---|---|---|
| | | | | | Leilani Richardson |
| a. REPORT | b. ABSTRACT | c. THIS PAGE | | | 19b. TELEPHONE NUMBER *(include area code)* |
| Unclassified | Unclassified | Unclassified | A | | (661) 275-5015 |



3 items enclosed

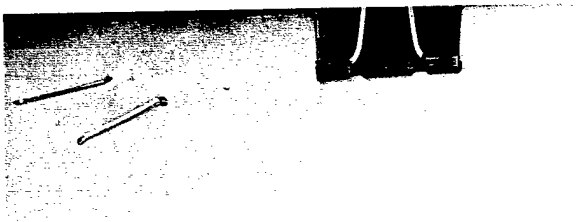

✓ DTS

ktr # = BMDO SBTR F0461-99-C-0005

MEMORANDUM FOR PRS (Contractor Publication)

9 September 1999

FROM: PROI (TI) (STINFO)

SUBJECT: Authorization for Release of Technical Information, Control Number: **AFRL-PR-ED-TP-FY99-0177**
Braunstein, M. and Duff, J. (Spectral Sciences); Electronic Structure and Dynamics of O(3P) + CO(1E+) Collisions

**Journal of Chemical Physics**

**(Statement A)**

Title: Electronic Structure and Dynamics of $O(^3P) + CO(^1\Sigma^+)$ Collisions

[Draft Manuscript 9/99]

M. Braunstein and J. W. Duff

*Spectral Sciences, Incorporated*
*99 S. Bedford Street, Suite # 7*
*Burlington, MA 01803*

Abstract:

The potential energy surfaces of the three lowest electronic triplet states of $CO_2$ which lead to $O(^3P)+CO(^1\Sigma^+)$, $^3A'$, $1^3A'$, and $2^3A''$, have been computed at the complete-active-space-self-consistent-field plus second-order perturbation theory (CASSCF-MP2) level with a modest G631+d basis. Potential energy surfaces are fit with a global functional form. The $^3A'$ state has a well 0.9 eV deep and the $1^3A''$ state has a 0.2 eV well with respect to the $O(^3P)+CO(^1\Sigma^+)$ dissociation threshold. The $^3A'$ and $1^3A''$ states are both bent at their minima and have a barrier at 0.2 eV and 0.3 eV above threshold, respectively. The $2^3A''$ state is mostly repulsive, and has a saddle at $C_{2v}$ geometries. We have run classical trajectory calculations for $O(^3P)+CO(^1\Sigma^+)$ collisions using these surfaces. Results agree well with available vibrational relaxation and oxygen atom exchange measurements except at low temperature. Comparisons are also made with measured vibrational excitation cross sections and infrared emission spectra of the nascent CO products at 3.4 eV collision energy. These results show a high degree of vibrational and rotational excitation with a nearly statistical population which is evident in a distinct spectral "band-head" signature. Analysis of the trajectories show that almost all collisions which lead to oxygen atom exchange and/or vibrational energy transfer occur when the $O(^3P)$ approaches the CO at OCO angles between $80^0$ and $140^0$, passes over the barrier and through the wells of the $^3A'$ and $1^3A''$ states, and interacts with the repulsive wall of the carbon end of the CO nearly perpendicular to the CO bond.

## I. INTRODUCTION

Collisions of $O(^3P)$ with $CO(^1\Sigma^+)$ have been measured by several authors in the context of vibrational relaxation of CO.[1,2] This process is a potentially important loss mechanism in the kinetics of the CO chemical laser, where the reaction O + CO produces vibrationally hot CO.[3] The vibrational relaxation of $CO(^1\Sigma^+)$ and other closed shell systems by $O(^3P)$ is extremely efficient, and is faster by several orders of magnitude than standard theories of translational to vibrational energy transfer (which assume only repulsive interactions) predict.[4] From symmetry considerations, there are only three electronic states of $CO_2$, all triplets, which lead to $O(^3P) + CO(^1\Sigma^+)$ and which play a role in this chemistry: a single $^3A'$ state and two $^3A''$ states. The nearby singlet states, which can only participate through weak spin-orbit interactions, lead to $O(^1D)$ and $CO(^1\Sigma^+)$, about two eV above $O(^3P)+CO(^1\Sigma^+)$. One of these five singlet states leads to the $^1\Sigma_g^+$ ground state of $CO_2$ about 5.5 eV below the $O(^3P) + CO(^1\Sigma^+)$ threshold, but the remainder are relatively high in energy and give rise to some of the complex $CO_2$ UV photoabsorption spectrum starting at about 1 eV above the $O(^3P)+CO(^1\Sigma^+)$ threshold.[5]

Experimental evidence of the three low-lying triplet states of $CO_2$ , which are spin-forbidden from the singlet ground state, is sparse. Isotopic exchange studies using $O^{18}+CO^{16}$ indicate a small barrier of about 0.25 eV.[6,7] Chemiluminescent recombination experiments with O+CO also suggest a low barrier.[8] Rebalais *et al.*[9] has tentatively assigned one of the flame bands of CO seen by Dixon[10] to one of these triplet states. More recently, Upschulte and Caledonia[11] have measured the cross section for vibrational excitation of $CO(^1\Sigma^+)$ by fast $O(^3P)$ at a collision energy of 3.4 eV (8 km/s) by monitoring the infrared radiation of the relaxing CO. Although rotational structure of the product CO was not resolved, their results show a high degree of CO vibrational excitation. There have been several *ab-initio* calculations of the triplet states aimed at understanding the complex $CO_2$ excitation spectrum and have mainly been done at the single geometry of the linear ground state.[12-18] McCurdy and McKoy[17] from an SCF equations of motion calculation assign two of these triplet states to peaks seen in the electron impact spectrum.[19] The early configuration-interaction calculation of Winter *et al.*[12] indicate that two of the triplet states may be bound with respect to the $O(^3P) + CO(^1\Sigma^+)$ limit, and have an equilibrium geometry of about $120^0$ and bond lengths slightly longer than the ground state. England *et al.*[13-16] explored the ordering of the triplet states near the $CO_2$ ground state linear geometry. Kelley and Thommarson[20] constructed a single "effective" potential surface for $O(^3P)$ +

$CO(^1\Sigma^+)$ collisions based on experimental measurements of the barrier height, and a well depth and geometry suggested by earlier *ab-initio* calculations. By adjusting the potential surface and carrying out classical trajectory calculations, they were able to reproduce the experimental data over a range of temperatures. Because of the approximate nature of their surface, however, it is not clear whether the correct dynamics have been captured in these calculations. Overall, the behavior of the triplet states in geometries leading to dissociation to $CO(^1\Sigma^+) + O(^3P)$ seems to be unexplored and it is these geometries which are important to vibrational relaxation, exchange, and excitation at energies from threshold up to about 5 eV.

To get a unified picture of $O(^3P)+CO(^1\Sigma^+)$ collisions, we have computed the potential energy surfaces of the three low-lying triplet states of $CO_2$ which lead to these products, $^3A'$, $1^3A''$, and $2^3A''$, at all geometries up to 5 eV above threshold. Our calculations were done using a complete-active-space-self-consistent field plus second-order perturbation theory (CASSCF-MP2) level of electron correlation with a modest G631+d basis set. We find that the $^3A'$ state is bound and has a well depth of 0.9 eV and barrier height of 0.2 eV with respect to the dissociation limit $O(^3P) + CO(^1\Sigma^+)$, and the $1^3A''$ state is also bound with a well depth of 0.2 eV and a barrier height of 0.3 eV. The third triplet state leading to $O(^3P) + CO(^1\Sigma^+)$, $2^3A''$, is mostly repulsive, and has a saddle in $C_{2v}$ geometries. We have fit the computed points for each of these surfaces to a functional form and performed classical trajectory calculations to compute vibrational relaxation and isotopic exchange rates and vibrational excitation cross sections over a range of conditions. The results agree well with measurements except at low temperatures. We find that the reaction dynamics are dominated by those collisions where the colliding atomic oxygen passes over the barrier and through the wells of the $^3A'$ and $1^3A''$ states and interacts with the inner repulsive wall of the carbon end of the CO at OCO angles between $80^0$ and $140^0$. This mechanism usually leads to excitation of high vibrational and rotational levels. At high collision energies, this leads to a distinctive infrared radiative "bandhead" signature of the nascent CO products. We also note that both reactive (exchange of oxygen atoms) and non-reactive mechanisms can lead to translational-to-rovibrational energy transfer. The importance of each of these mechanisms is different for each of the triplet states, with the $^3A'$ state favoring non-reactive exchange and the two $^3A''$ states favoring reactive exchange as a mode of energy transfer.

The paper will proceed as follows: Section II will describe the method of *ab-initio* calculations, and present the major features of the surfaces. Section III will describe how the *ab-initio* surfaces are fit to a functional form and present the results of this fit. In Section IV we will present results of our calculations for vibrational relaxation, isotopic exchange and vibrational excitation and compare these to available experimental measurements. In Section V we discuss the energy transfer mechanism in more detail and in Section VI give conclusions.

## II. ELECTRONIC STRUCTURE CALCULATIONS

As we are interested in accurately computing complete potential surfaces (including excited states) for $O(^3P)$ + $CO(^1\Sigma^+)$ collisions, it is important to choose a method which is flexible and accurate enough to describe potential wells, barriers, and dissociation to open shell fragments. Quasidegenerate perturbation theory (QDPT) with multiconfiguration self-consistent-field (MCSCF) reference functions developed by Nakano is a multi-state, multi-reference method which combines the wide applicability of MCSCF methods with the efficiency of perturbation theory in capturing the important contributions of the correlation energy.[21] It has been shown to be comparable in accuracy to multireference single and double excitation configuration interaction (CI) and full CI treatments for some test cases at a computational savings. The calculations reported here use this method as implemented in the GAMESS suite of programs which include perturbation theory contributions through second order (CASSCF-MP2).[22]

A complete-active-space-self-consistent-field (CASSCF) wave function was constructed for the lowest $^3A'$ state and the two lowest $^3A''$ states of $CO_2$. Table I shows the active space orbitals and main configurations of the CASSCF wave functions which consisted of all possible excitations of 12 electrons among 10 orbitals, amounting to 10,374 configuration state functions (CSFs) for the $^3A'$ state and 10,416 CSFs for the two $^3A''$ states. These excitations included the valence bonding and anti-bonding orbitals to insure a proper description of dissociation. For these calculations a modest G631+d basis was used. The diffuse functions were included to describe any Rydberg-valence mixing which is known to occur near linear geometries.[13-16] For reference, the CASSCF and MP2 energies of the ground state singlet of $CO_2(^1\Sigma_g^+)$ and lowest $^3A'$ and $^3A''$ states are shown in Table II at the ground state experimental equilibrium geometry along with the results of Winter *et al.*[12] using a relatively small CI calculation. Table III shows the calculated vertical and adiabatic excitation energies of the lowest $^3A'$ and $^3A''$ states along with several other *ab-initio* results. The

results agree particularly well with England *et al.*[13] which have a comparable basis and level of electron correlation.

The main features of the surfaces can be seen in Fig. 1, which shows results of the present calculations for the ground singlet state of $CO_2$, $^1A'$, the lowest $^3A'$ state and two lowest $^3A''$ states at geometries leading to dissociation. Here the OCO bond angle is $120^0$, one of the CO bond lengths is fixed at 1.2 Å, and the energy is shown as a function of the second CO length. As discussed further below, there can only be three states, all triplets, which lead to $O(^3P) + CO(^1\Sigma^+)$ and these are the $^3A'$, $1^3A'$ and $2^3A''$ states. The $^3A'$ state has a well 0.9 eV below threshold and a barrier about 0.2 eV above threshold. The $1^3A''$ state has a shallower well of about 0.2 eV and a similar barrier height as the $^3A'$ state. The $2^3A''$ state is mostly repulsive and has a saddle in $C_{2V}$ geometries. (We note that Herzberg's discussion of the lowest $CO_2$ triplet potential energy surfaces apparently includes only this last mostly repulsive state and not the two others.[23] This ambiguity has probably led to an underestimation of the O+CO collision cross section in a previous study.[24]) At its minimum the ground singlet state is about 5.5 eV below the $O(^3P) + CO(^1\Sigma^+)$ threshold. It is interesting that the ground singlet state ($^1A'$) crosses these triplet states and leads to the higher dissociation limit of $O(^1D) + CO(^1\Sigma^+)$. There are four other singlet states leading to this limit. At linear geometries some of these give rise to the rich UV photoabsorption spectrum. The next highest dissociation limit which allows triplet states of $CO_2$ is the $O(^3P)+CO(a^3\Pi)$ limit which is about 6 eV above the $O(^3P)+CO(^1\Sigma^+)$ threshold. We would expect therefore that $CO_2$ triplet states leading to this higher threshold do not play a significant role at the collision energies examined in this study.

By symmetry, there are three states which can lead to $O(^3P) + CO(^1\Sigma^+)$: $^3A'$, $1^3A''$, and $2^3A''$. As we are mainly interested in geometries leading to dissociation and to simplify keeping track of these states and other possible excited triplet states, all calculations were done in $C_s$ symmetry, finding the lowest triplet A' and two lowest triplet A'' roots. It is known from earlier work that in $D_{\infty h}$ geometries many $CO_2$ triplet states either form degenerate pairs or come close in energy.[12-18] But according to these studies and the present work, this occurs at energies 3 to 5 eV above threshold, and so we would expect other triplet states to play a minimal role in the chemistry of interest. In fact, we have found that the second $^3A''$ state contributes to the dynamics only at energies above 3eV above threshold, and the contribution is minor. Likewise, we have found that the second excited $^3A'$ state occurs high enough in energy that it too does not influence the dynamics. Therefore, we are

confident that the lowest $^3$A' and two lowest $^3$A'' state surfaces will be adequate to describe the collision dynamics from threshold to 4 or 5 eV.

We have computed CASSCF-MP2 energies at about 320 unique points to determine the potential energy surfaces of the lowest $^3$A' and two lowest $^3$A'' states. These were computed at OCO bond angles of $20^0$, $40^0$, $60^0$, $90^0$, $100^0$, $110^0$, $120^0$, $130^0$,$150^0$, and $175^0$, and at bond lengths between 0.8 Å and 5 Å at increments ranging from 0.1 Å to 0.3 Å. These calculations were used to fit the potential surfaces of each of these states which is described in the next section. Extra calculations were done on a finer grid to determine properties near the minimum and barrier of the lowest $^3$A' and $^3$A'' states. Table IV gives the calculated minimum and barrier geometries and the vibrational frequencies of these states. Both these states have bent $C_{2v}$ minimum geometries, where they become $^3B_2$ and $^3A_2$ states, respectively. The $^3$A' state has a well depth of 0.94 eV and the $^3$A'' state has a well depth of 0.22 eV which just supports one bound vibrational state. These results are consistent with earlier calculations of Winter *et al.*[12] About 30 additional points were computed with one of the CO bond distances set to 5 Å to find the *ab-initio* diatomic CO($^1\Sigma^+$) potential within this computational scheme.

## III. POTENTIAL ENERGY SURFACE FITS

The CASSCF-MP2 energies for the lowest $^3$A' state and two lowest $^3$A'' states were globally fit with the method of Aguado and Paniagua.[25] Here the potential energy function for the triatomic $CO_2$ for each of the states is written as a sum of two-body and three body terms:

$$V_{OCO} = V^{(2)}_{CO}(R1) + V^{(2)}_{OO}(R2) + V^{(2)}_{CO}(R3) + V^{(3)}_{OCO}(R1, R2, R3). \quad (1)$$

The monotonic terms here have been omitted because all reaction channels for O($^3$P) + CO($^1\Sigma^+$) correlate with the atoms in their ground electronic states. The two body terms for CO and $O_2$ have been determined from fits to the following polynomial potential form

$$V^{(2)}_{AB}(R_{AB}) = \frac{c_0 e^{-\alpha_{AB} R_{AB}}}{R_{AB}} + \sum_{i=1}^{N} c_i \rho^i_{AB}, \quad (2)$$

where the polynomial variables ρ are given by,

$$\rho_{AB} = R_{AB} e^{-\beta^{(i)}_{AB} R_{AB}}, \quad (3)$$

and $l=2$ for these two-body terms. This leaves the linear parameters $c_i$, $i=0,1,...N$ and nonlinear parameters $\alpha$ and $\beta$ to be determined from fitting the diatomic fragment potentials. For the CO diatomic fragments, we used the *ab-initio* points described in the previous section. With $N=3$ a non-linear least squares method based on Ref. 26 yielded a fit of less than 0.001 eV root mean square error obtained for points within 5 eV of $CO(^1\Sigma^+)$ equilibrium geometry. Overall, agreement with the RKR curve for CO at these energies is excellent except for a slight shift in the CO equilibrium bond distance from the experimentally determined equilibrium value of 1.128 Å to the *ab-initio* value of 1.150 Å. Since the ground state $O_2(^3\Sigma_g^-)$+$C(^3P)$ channel occurs about 6 eV above the $O(^3P)$ + $CO(^1\Sigma^+)$ threshold, we thought it adequate to use a fit to the experimentally determined RKR potential surface of the $O_2(^3\Sigma_g^-)$ fragment for the $O_2$ diatomic potential term with $N=4$. The two-body terms are listed in Table V.

The three-body term, $V^{(3)}_{oco}(R1,R2,R3)$, is a polynomial in $\rho$ as in Eq. 3 above except with $l=3$,

$$V^{(3)}_{OCO}(R1,R2,R3) = \sum_{i,j,k}^{M} d_{ijk}\rho^i_{CO}\rho^j_{OO}\rho^k_{CO}. \qquad (4)$$

There are constraints on the allowed values of $i,j$, and $k$ in general and additional symmetry constraints imposed by the $AB_2$ symmetry of this system. We used the same non-linear least squares method to fit the three-body potential terms resulting from subtraction of the fitted two-body terms discussed above from the total *ab-initio* energies for each of the surfaces. No explicit weighting was used, but the density of *ab-initio* points was concentrated near the wells, barriers and along the minimum reaction path of the two-lowest states. An initial fit with $M=4$ was found for each of the states, and the value of $M$ was increased. It was found that as the value of $M$ increased beyond 6 or 7, unphysical oscillations and very deep wells would begin to occur in regions where there were none or very few calculated *ab-initio* points. These regions were very high in energy (greater than 5 eV) and usually occurred at small OCO bond angles. Extremely good fits were obtained if bond angles greater than $150^0$ and less than $60^0$ were excluded even with low $M$ values. Including angles greater than $150^0$ and less than $60^0$ required using larger values of $M$ which often introduced the very deep unphysical wells mentioned previously, or created a bad fit near in the "reaction path" region. By estimating a few high energy points (>5 eV above threshold) at small bond angles which "pinned" the potential, a compromise was reached where a root-mean-square error of less than 0.1 eV was obtained for the well and barrier regions, and generally a 0.2 eV error was achieved for the

small and large angle high energy regions, with a value of $M=6$ for the $^3A'$ state and lowest $^3A''$ state and a value of $M=5$ for the second $^3A''$ state. Table VI shows the values of the three-body linear and nonlinear parameters for these states of $CO_2$ obtained in this way.

For these fits, care was taken to assure that there were no spurious "holes" in the potential that would affect our classical trajectory calculations below 5 eV. We do note however that a good fit required that at very small OCO bond angles some deep wells do occur. But these are in regions which are not allowed classically, and are isolated enough that they could be removed easily with a small *ad-hoc* modification of the fit.

The potential energy surfaces for each of the three states at a number of fixed bond angles are shown in Fig. 2. For the $^3A'$ and $1^3A''$ state the bent well regions and barrier regions are clearly evident. The $2^3A'$ state is mostly repulsive, and has a saddle near $100^0$. Figure 3 shows polar potential plots of these states for a fixed CO bond distance of 1.15 Å, the *ab-initio* value of $r_e$ for the CO fragment. In these plots the carbon atom is located at the origin and one of the oxygen atoms is at –1.15 Å. The values of the contours correspond to energies of the different bond angles and distances of the approaching oxygen atom during a collision. The angular dependence of the well and barrier is clearly seen for the two lowest states. The wells appear at OCO angles of around $125^0$ for each of the $^3A'$ and lowest $^3A''$ states and the barrier is lowest at slightly smaller angles. Even the upper $2^3A''$ favors these bent geometries. These features have implications for the collision dynamics which will be discussed in the following sections.

## IV. QUASI-CLASSICAL TRAJECTORY CALCULATIONS: COMPARISONS WITH EXPERIMENTAL DATA

Using the three potential energy surfaces described in the previous section, quasi-classical trajectory (QCT) vibrational relaxation and exchange rates and excitation cross sections for $O(^3P)+CO(^1\Sigma^+)$ collisions have been computed using standard Monte-Carlo techniques.[27] For these calculations, each state was considered independently and its contribution to each process was multiplied by the statistical weight of 1/3, due to electronic degeneracy. We feel that an independent (non-interacting) treatment of the dynamics is justified since the calculated $^3A'$ and lowest $^3A''$ adiabatic states which dominate the collision dynamics below 5 eV cannot interact in $C_s$ geometries (where most of the collision dynamics take place) by symmetry, nor can they interact in $C_{2V}$

geometries where they become $^3B_2$ and $^3A_2$ states, respectively. They can only possibly interact in $D_{\infty h}$ geometries which occur at higher energies. The $2^3A''$ state can interact with the $1^3A''$ state, but these states only come close at energies high above threshold, and at dissociation where they become degenerate. For the vibrational relaxation calculations, the initial rotational and translational distributions were chosen from a Boltzmann distribution at a specified temperature and the v=1 level of CO was initially populated. The calculated exchange processes used initial translation, vibration, and rotation populations from a Boltzmann distribution at a specified temperature and only the v=0 level of CO was initially populated. The excitation cross sections were calculated at a fixed collision velocity from an initial CO population in v=0 and a rotational population from a Boltzmann distribution at $300^0$ K, meant to simulate a fast O atom molecular beam measurement. For the relaxation and exchange calculations, 30,000 trajectories per temperature per electronic state were used. For the excitation calculations, 10,000 trajectories per energy per electronic state were used.

Figure 4 shows the calculated vibrational relaxation rates as a function of inverse temperature along with the data of Center[1] from shock-tube measurements at high temperature, the data of Lewittes *et al.*[2] from low temperature measurements, and the classical trajectory results of Kelley and Thommarson[20] using an empirically adjusted "effective" potential energy surface. The present calculations were done at temperatures of $300^0$, $500^0$, $1000^0$, $2000^0$, and $4000^0$. There is good agreement between the present results and the measurements at high temperatures, and about an order of magnitude difference with the low temperature results of Lewittes *et al.*[2] More measurements at intermediate temperatures may help clarify these differences. The results of Kelley and Thomarrson[20] under-estimate the experimental results of Lewittes *et al.*[2] as well, but tend to over-estimate the high temperature rates. We note that the same surface of Kelley and Thomarrson without the bending potential resulted in unphysically high rates, and that their final surface resulted from estimating a bending potential to match the measured rates. It therefore seems unlikely between their results and the present ones that the low temperature measurements can result from any fine adjustment of the triplet potential surfaces and probably arises from another mechanism. It is possible that the enhanced rate at low temperature could be caused by interaction of the ground singlet state of $CO_2$ (or other nearby singlet states) with the two lowest triplet states which can occur through spin-orbit mixing. As shown in Fig. 1 these states cross in the barrier region. Quantum effects not considered here may also contribute to the low temperature rate, although we expect

these to be minor. We note that at very low temperatures the vibrational relaxation rate is dominated by contributions from the $^3$A' state. At 4000$^0$, the $^3$A'' contribution is about half that of the $^3$A' state. The contribution from the second $^3$A'' is negligible through this temperature range. Vibrational relaxation can occur through reactive (exchange of O atom) and non-reactive collisions and each contributes about equally to the rate. Figure 5 shows the calculated oxygen atom exchange rates as a function of inverse temperature along with the experimental results of Jaffe and Klein[7] and Garnett *et al.*[6] Agreement with experiment is good even at low temperature. This suggests that the present approach gives the correct low-energy behavior for reactive O + CO collisions and contrasts with the vibrational relaxation results.

Figure 6 shows calculated vibrational excitation cross sections for CO(v=0) as a function of collision energy from 0.5 to 4 eV. Calculations were done at 0.5 eV, 1.0 eV, 2.0 V, 3.0 eV, and 4.0 eV. Collisions at these high energies are important in space applications, where at orbital altitudes (greater than ~250 km) O($^3$P) is the dominant species. The dashed curve shows the calculated v=0 v'=1 cross section. The solid curve shows the calculated weighted sum of cross sections: $\sigma$(v=0 1)+2$\sigma$(v=0 2)+3$\sigma$(v=0 3) + ... Also shown is the data point at 8 km/s (3.4eV) from the fast O($^3$P) measurements of Upschulte and Caledonia.[11] These authors measured the infrared radiation from vibrationally excited CO resulting from O+CO collisions but were not able to separate contributions from individual vibrationally excited states of the CO product. By making an approximation for the vibrationally excited state lifetimes, they converted the measured total radiation to the weighted sum of vibrational excitation cross sections defined above. The theoretical results are about an order of magnitude above the experimental measurement, which is surprising since there was good agreement with the high temperature vibrational relaxation measurements. We note, however, that the time versus intensity plots of excited state products in Ref. 11 show falloffs much shorter than excited state lifetimes. We suspect, therefore, that vibrationally excited CO molecules are colliding out of the field of view of the detector before they can radiate; and the experimental measurement is actually a lower bound for this summed cross section.

Figure 7a shows the calculated infrared emission spectra of the nascent distribution of excited CO at an O+CO collision energy of 3.4 eV. The resolution is 5 cm$^{-1}$ and only quantum transitions to the next lowest vibrational state are included. The labeled peaks are locations of band heads to different final vibrational levels of CO. Very high vibrational excitation is evident. The band heads

arise from excitation to high j (j=50-100) R branches of vibrationally excited CO and make a distinctive spectral signature. Figure 7b shows the same calculated spectra but degraded in resolution to match the data of Upschulte and Caledonia[11] which are also shown. The experimental spectra were obtained at pressures which correspond to ~5 collision conditions in order to achieve good signal to noise so a direct comparison is not possible. But the agreement suggests that the calculations are at least qualitatively correct.

## V. ENERGY TRANSFER MECHANISMS

### A. CROSS SECTION COMPONENTS

In this section, the calculated cross sections are broken down into their constituent components (reactive, non-reactive, electronic, vibrational and rotational) to investigate the mechanism for translation to rovibrational energy transfer. Excitation cross sections are analyzed, but the general trends carry over to exchange and vibrational relaxation as well. Figure 8 shows the O+CO excitation cross sections at different energies to final vibrational states of CO. Between 1 eV and 2 eV the excitation to higher vibrational levels begins to "hang-up" at a constant level, leading to very high vibrational excitation. This suggests that perhaps for energies less than ~0.5 eV many collisions do not reach the wells of the two lower triplet states, and that above ~0.5 eV access to this inner region where energy exchange is efficient is more easily allowed. Figure 9 shows the electronic components of the cross section to different final vibrational levels of CO at a collision energy of 3eV. For vibrational excitation and vibrational energy transfer in general, the $^3A'$ and lowest $^3A''$ state track each other, with the $^3A'$ state usually a factor of 2 greater in magnitude. The two potential energy surfaces are similar, the main difference being the deeper well of the $^3A'$ state. At these energies above the barrier the fact that their contributions are similar is not that surprising. The second $^3A''$ state is qualitatively different from the lower triplet states. It is mostly repulsive with no bound well and contributes much less to the overall cross section. Vibrational excitation of this $^3A''$ state falls off much faster than the other electronic states.

Translation to vibrational energy transfer can proceed with and without the exchange of oxygen atoms. Figure 10 shows the ratio of reactive to non-reactive cross sections for excitation v=0 v'=1 of CO as a function of collision energy for each of the electronic states. For the two $^3A''$ states the reactive channel is greater, while for the $^3A'$ state the nonreactive channel is greater. This is

surprising because the major difference between the $^3A'$ state and the $^3A''$ state is the well depth, which should have little effect on the dynamics at these collision energies. As will be discussed later, vibrational energy transfer appears to be dominated by collisions where the approaching oxygen travels over the barrier and comes close to the target CO. We believe the preference for reactive collisions accompanying vibrational energy transfer in the lower $^3A''$ comes from the shape of the repulsive wall inside the barrier. Part of this repulsive wall is shown for the $^3A'$ and $^3A''$ states in Fig. 11, where the target CO molecule bond distance is fixed, and the oxygen atom approaches at a fixed bond angle. The steepness (derivative) of the wall for each state is similar, but the repulsive wall is displaced to smaller CO bond distances for the $^3A'$ state, partly due to the presence of the deeper and wider well. The placement of the repulsive wall of the $^3A''$ state corresponds closely to the equilibrium geometry of the exchange product CO and it appears it is this feature which makes the $^3A''$ surface more "reactive". It is interesting to note also that the ratio of reactive to nonreactive cross sections summed over all electronic states is close to 1 for the entire range of collision energies. This is something that could be verified experimentally using $O^{18}$ as a reactant, which should yield similar results. In Fig. 12 the cross sections for excitation to different final vibrational levels for each electronic state is broken down into reactive and non-reactive components. For vibrational energy transfer, the preference for reactive collisions accompanying excitation is generally true for the two $^3A''$ states, except for the first $^3A''$ state at very high vibrational excitation, while the non-reactive channel is dominant for the $^3A'$ for all vibrational levels. Vibrationally elastic collisions are all dominated by the non-reactive channel. When translation-to-vibrational energy transfer does occur, therefore, it is usually accompanied by a high degree of reactive exchange which suggests that the reactant oxygen atom must get close to the target CO.

Figure 13 shows rotational energy distributions at 3 eV for excitation from v=0 to v'=0 and v'=1 including reactive and non-reactive channels summed over all three electronic states. For the v'=1 level the degree of rotational excitation becomes quite high (j~100) and accommodates all the available collision energy. Population of these high-j states gives rise to the band-head signature of the infrared spectrum shown earlier. Suprisal plots[28] of these distributions are also shown and indicate a nearly statistical distribution of rotational states for excitation to v'=1, except for very low j. The very low-j population may be a reflection of the fact that the maximum impact parameter in

the classical trajectory calculations was chosen mostly on the basis of determining accurate v'>0 populations, and so may not be as accurate for vibrationally elastic collisions. The component electronic, reactive, and non-reactive rotational distributions were similar.

### B. REPRESENTATIVE CLASSICAL TRAJECTORIES

From examination of the trajectories it is clear that almost all collisions which lead to oxygen atom exchange or vibrational energy transfer occur when the approaching oxygen atom passes over the barrier at OCO angles between 80 and 140 degrees. This is true for all three electronic surfaces so that these collisions occur mostly with the approaching oxygen interacting with the inner repulsive wall at the carbon end perpendicular to the CO bond. This in part leads to efficient population of high-j rotational and high-v vibrational states, and is similar to behavior seen in fast H atom collisions with CO.[29,30] Figure 14 shows the point of closest approach of the colliding oxygen atom which lead to non-reactive vibrational energy transfer for the $^3A'$ state for the process $O(^3P)+CO(^1\Sigma^+)(v=0\ v')$ at a collision energy of 3eV superimposed on a polar plot of the potential energy surface as in Figure 3. These points, drawn from a random set of trajectories, collect past the barrier region in the inner wall of the potential surface. Also shown are the locations of the reacting oxygen atom at the geometry of the "tightest collision complex" for reactive (oxygen atom exchange) collisions which lead to vibrational energy transfer where the summed bond lengths $r_{CO}+r_{OO}+ r_{CO}$ is a minimum. All these locations also collect past the barrier, so that "reactive" collisions seem, at least initially, to follow the same mechanism as non-reactive vibrational energy transfer collisions. Examination of the reactive and non-reactive trajectories at 3 eV on the $^3A'$ surface which lead to vibrational energy transfer show in most cases that these collisions happen quickly, usually in less than a vibrational period. However, in a significant number of vibrational energy transfer trajectories the approaching oxygen atom appears to become "caught" in the inner well region for a duration of several vibrational periods. When this happens the OCO bond angle will stay near ~$90^0$-$130^0$. At lower collision energies the number of these kind of trajectories becomes more pronounced. Similar results hold for the other two potential energy surfaces.

## VI. CONCLUSIONS

We have computed the potential energy surfaces of the three lowest triplets of $CO_2$ at the CASSCF-MP2 level of theory with a modest G631+d basis and fit these global surfaces to a

functional form. The lowest $^3A'$ state has a well 0.9 eV deep and the lowest $^3A''$ state has a 0.2 eV well with respect to the $O(^3P)+CO(^1\Sigma^+)$ dissociation threshold. Both are bent at their minima and have a barrier about 0.3 eV above threshold. The second $^3A''$ state is mostly repulsive. Classical trajectory calculations on these surfaces agree well with available vibrational relaxation and oxygen atom exchange measurements of $O(^3P) + CO(^1\Sigma^+)$ collisions except at low temperature. Calculated cross sections at 3.4 eV collision energy for vibrational excitation of CO are about an order of magnitude above the single measured data point for this process. Comparison of the emission spectra of the nascent CO product distributions are in fair agreement, and show a high degree of vibrational and rotational excitation. This population of high-j states accompanying reactive and non-reactive vibrational excitation is nearly statistical, and is evident in the infrared "band-head" signature of the CO products. Analysis of the trajectories show that almost all collisions which lead to oxygen atom exchange or vibrational energy transfer occur when the approaching oxygen atom passes over the barrier and through the wells of the lowest two triplets at OCO angles between $80^0$ and $140^0$, leading to collisions where the oxygen interacts with the inner repulsive wall of the carbon end of the CO bond. Usually the oxygen atom initially stays in the inner well region less than a vibrational period, but in a number of trajectories the approaching oxygen atom remains for many vibrational periods.

## Acknowledgments

The authors wish to thank Dr. L. Bernstein and Dr. W. Dimpfl of Spectral Sciences, Inc. for several helpful technical discussions. The authors also acknowledge Capt. D. Ziegler and Mr. T. Smith of the Air Force Research Laboratory for oversight and encouragement of this work. This work was supported by a small business innovative research (SBIR) grant from the Ballistic Missile Defense Organization (BMDO) contract F04611-99-C-0049.

## References

1. R. E. Center, *J. Chem. Phys.* **58,** 5230 (1973).

2. M. E. Lewittes, C. C. Davis, and R. A. McFarlane, *J. Chem. Phys.* **69,** 1952 (1978).

3. G. Hancock, C. Morley, and I. W. M. Smith, *Chem. Phys. Lett.* **12**, 193 (1971).

4. C. Park, "Nonequilibrium Hypersonic Aerothermodynamics", Wiley Interscience, New York (1990), pp. 57-60.

5. E. C. Y. Inn, K. Watanabe, and M. Zelikoff, *J. Chem. Phys.* **21**, 1648 (1953).

6. S. H. Garnett, G. B. Kistiakowsky, and B. V. O'Grady, *J. Chem. Phys.* **51,** 84 (1969).

7. S. Jaffe and F. S. Klein, *Trans. Faraday Soc.* **62,** 3125 (1966).

8. M. A. A. Clyne and B. A. Thrush, *Proc. Roy. Soc. London Ser. A* **269**, 404 (1962).

9. J. W. Rabalais, J. M. McDonald, V. Scherr, and S. P. McGlynn, *Chemical Reviews* **71,** 73 (1971).

10. R. N. Dixon, *Proc. Roy. Soc. Ser. A* **275,** 431 (1963).

11. B. L. Upschulte and G. E. Caledonia, *J. Chem. Phys.* **96**, 2025 (1992).

12. N. W. Winter, C. F. Bender, and W. A. Goddard III, *Chem. Phys. Lett.* **20,** 489 (1973).

13. W. B. England and W. C. Ermler, *J. Chem. Phys.* **70,** 1711 (1979).

14. W. B. England, D. Yeager, and A. C. Wahl, *J. Chem. Phys.* **66,** 2344 (1977).

15. W. B. England, W. C. Ermler, and A. C. Wahl, *J. Chem. Phys.* **66,** 2336 (1977).

16. W. B. England, B. J. Rosenberg, P. J. Fortune, and A. C. Wahl, *J. Chem. Phys.* **65,** 684 (1976).

17. C. W. McCurdy, Jr. and V. McKoy, *J. Chem. Phys.* **61,** 2820 (1974).

18. P. S. Julienne, D. Neumann, and M. Kraus, *J. Atmos. Sci.* **28,** 833 (1971).

19. V. V. Foo, C. E. Brion, and J. B. Hasted, *Proc. Roy. Soc. London Ser A* **322**, 535 (1971).

20. J. D. Kelley and R. L. Thommarson, *J. Chem. Phys.* **66,** 1953 (1977).

21. H. Nakano, *J. Chem. Phys.* **99,** 7983 (1993).

22. M. W. Schmidt, K. K. Baldridge, J. A. Boatz, S. T. Elbert, M. S. Gordon, J. H. Jensen, S. Koseki, N. Matsunaga, K. A. Nguyen, S. J. Su, T. L. Windus, M. Dupuis, J. A. Montgomery, *J. Comput. Chem.* **14,** 1347 (1993).

23. G. Herzberg, "Molecular Spectra and Molecular Structure III. Electronic Spectra and Electronic Structure of Polyatomic Molecules", Van Nostrand Reinhold Co., pp. 429-431 (1966).

24. M. J. Redmon, L. T. Redmon, and B. C. Garret, "Collision Excitation Cross Sections", Air Force Rocket Propulsion Laboratory, Report ~~F04611-82-C-0041~~ AFRPL-TR-84-030, Edwards Air Force Base, CA August, 1984.

25. A. Aguodo and M. Paniagua, *J. Chem. Phys.* **96**, 1265 (1992).

26. D. W. Marquardt, *J. Soc. Industrial and Applied Math.* **11**, 431 (1963).

27. D. G. Truhlar and J. T. Muckerman, "Atom-Molecule Collision Theory", ed. R. B. Bernstein, Plenum Press, New York, p. 505 (1979).

28. R. D. Levine and R. B. Bernstein, "Molecular Reaction Dynamics and Chemical Reactivity", Oxford University Press, New York, pp. 260-270 (1987).

29. G. K. Chawla, G. C. Mcbane, P. L. Houston, and G. C. Schatz, *J. Chem. Phys.* **88,** 5481 (1988).

30. G. C. Mcbane, S. H. Kable, P. L. Houston, and G. C. Schatz, *J. Chem. Phys.* **94,** 1141 (1991).

Table I. Orbital space and main configurations for CASSCF wave functions of $CO_2$ for the ground state($^1\Sigma_g^+$), lowest $^3$A' state and two lowest $^3$A'' states. Orbitals not shown are considered core orbitals and are all doubly occupied: [core]=$1\sigma_g^2 1\sigma_u^2 2\sigma_g^2 3\sigma_g^2 2\sigma_u^2$.

| orbital | 6 | 7 | 8 | 9 | 10 | 11 | 12 | 13 | 14 | 15 |
|---|---|---|---|---|---|---|---|---|---|---|
| $C_s$ | a' | a'' | a' | a' | a'' | a' | a' | a'' | a' | a' |
| $C_{2v}$ | $4a_1$ | $1b_1$ | $5a_1$ | $3b_2$ | $1a_2$ | $4b_2$ | $6a_1$ | $2b_1$ | $5b_2$ | $7a_1$ |
| $D_{\infty h}$ | $4\sigma_g$ | $1\pi_u$ | $1\pi_u$ | $3\sigma_u$ | $1\pi_g$ | $1\pi_g$ | $2\pi_u$ | $2\pi_u$ | $4\sigma_u$ | $5\sigma_g$ |
| | | | | | $^1$A' ($^1\Sigma_g^+$) | | | | | |
| | 2 | 2 | 2 | 2 | 2 | 2 | 0 | 0 | 0 | 0 |
| | | | | | $^3$A' | | | | | |
| | 2 | 2 | 2 | 2 | 2 | 1 | 1 | 0 | 0 | 0 |
| | | | | | $1^3$A'' | | | | | |
| | 2 | 2 | 2 | 2 | 1 | 2 | 1 | 0 | 0 | 0 |
| | | | | | $2^3$A'' | | | | | |

| | | | | | | | | | | |
|---|---|---|---|---|---|---|---|---|---|---|
| | 2 | 2 | 2 | 2 | 1 | 0 | 0 | 0 | 1 | 0 |

Table II. Electronic energies in a.u. at the equilibrium geometry of the ground state $r_1=r_2=1.16$ Å, $\theta=180^0$, for the ground singlet state and the two lowest triplet states of $CO_2$.

| | | $^1A'(^1\Sigma_g^+)$ | $^3A'$ | $^3A''$ |
|---|---|---|---|---|
| present work | CASSCF | -187.809605 | -187.482789 | -187.459231 |
| | MP2 | -188.108205 | -187.805379 | -187.783404 |
| | | | | |
| Winter *et al.* Ref. 12 | CI | -187.6868 | -187.4167 | -187.3990 |

Table III. Vertical ($T_v$) and adiabatic ($T_e$) excitation energies in eV for the two lowest triplet states of $CO_2$. Main entries are computed with respect to the calculated energy of the ground state singlet determined at the experimental equilibrium geometry. Entries in parenthesis are with respect to the calculated CASSCF-MP2 $O(^3P)+CO(^1\Sigma^+)$ dissociation limit of –187.919703 a.u. at $r_{CO}=1.15$ Å.

| | | $T_v$ | $T_v$ | $T_e$ | $T_e$ |
|---|---|---|---|---|---|
| | | $^3A'$ | $^3A'$ | $^3A''$ | $^3A''$ |
| present results | CASSCF-MP2 | 8.23 (8.68) | 8.84 (9.28) | 4.19 (4.63) | 4.91 (5.35) |
| England *et al.* Ref. 13 | MC-CI | 8.65 | 8.86 | | |
| England *et al.* Ref. 15 | SCF | 8.10 | 8.70 | | |
| Winter *et al.* Ref. 12 | CI | 7.35 | 7.83 | 3.7 | 4.1 |

| | | | | | |
|---|---|---|---|---|---|
| McCurdy and McKoy Ref. 17 | SCF-EOM | 7.35 | 8.06 | | |

Table IV. Properties of the calculated $^3A'$ and $1^3A''$ states of $CO_2$. Well depths and barrier heights are with respect to the calculated $O(^3P)+CO(^1\Sigma^+)$ dissociation limit. For both states the well is a minimum at $C_{2v}$ geometries where $r_1=r_2$, and the barrier occurs at $C_s$ geometries.

| | $^3A'$ ($^3B_2$) | $^3A''$($^3A_2$) |
|---|---|---|
| potential well | | |
| $r_e$ | 1.26 Å | 1.27 Å |
| $\theta_e$ | $118^0$ | $127^0$ |
| $D_e$ | 0.94 eV | 0.22 eV |
| $\omega_1$ | 1,110 $cm^{-1}$ | 880 $cm^{-1}$ |
| $\omega_2$ | 540 $cm^{-1}$ | 580 $cm^{-1}$ |
| $\omega_3$ | 1,310 $cm^{-1}$ | 1,040 $cm^{-1}$ |
| barrier | | |
| $r_1$ | 1.16 Å | 1.16 Å |
| $r_2$ | 2.0 Å | 1.85 Å |
| $\theta$ | $112^0$ | $122^0$ |
| barrier height | 0.2 eV | 0.3 eV |

Table V. Two body terms of the $^3A'$, $1^3A'$, and $2^3A''$ potential energy surfaces. All coefficients are in a.u.

| | |
|---|---|
| Two body terms $V^{(2)}_{CO}$ | |

| i | $c_i$ |
|---|---|
| 0 | 8.6610 (02) |
| 1 | -2.0892 (01) |
| 2 | -4.5109 (01) |
| 3 | -1.0380 (03) |
| $\alpha_{CO}$ | 4.5276 (00) |
| $\beta^{(2)}_{CO}$ | 1.4939 (00) |
| Two-body term $V^{(2)}_{OO}$ | |
| i | |
| 0 | 6.9872 (03) |
| 1 | -7.0287 (-02) |
| 2 | 1.3604 (01) |
| 3 | -5.3808 (03) |
| 4 | 2.3658 (04) |
| $\alpha_{OO}$ | 7.5246 (00) |
| $\beta^{(2)}_{OO}$ | 1.7299 (00) |

Table VI. Three body terms, $V^{(3)}_{OCO}$, for the $^3A'$, $1^3A''$, and $2^3A''$ states of $CO_2$. All coefficients are in a.u. and $d_{ijk}=d_{kji}$. For the $^3A'$ and $1^3A''$ states *M=6*. For the $2^3A''$ state, *M=5*.

| | $^3A'$ | $1^3A''$ | $2^3A''$ |
|---|---|---|---|
| i j k | $d_{ijk}$ | $d_{ijk}$ | $d_{ijk}$ |
| 101 | 1.4053 (03) | 1.3349 (03) | 1.6349 (03) |
| 110 | 7.6464 (02) | -1.7795 (02) | 4.6540 (03) |

| | | | |
|---|---|---|---|
| 111 | -1.1766 (04) | -5.0575 (04) | -3.9843 (04) |
| 120 | -1.0466 (04) | 2.5297 (04) | 2.8737 (04) |
| 201 | 5.6554 (03) | 1.0890 (04) | -8.5622 (03) |
| 210 | -5.4682 (03) | 1.0033 (04) | -9.9447 (04) |
| 121 | -2.1786 (05) | 3.8667 (05) | 2.9063 (06) |
| 130 | -3.5576 (05) | -4.9268 (05) | -1.0182 (06) |
| 202 | -5.3779 (03) | 1.7707 (04) | 3.2658 (05) |
| 211 | 1.8977 (05) | 5.0046 (05) | -4.3917 (05) |
| 220 | 1.2656 (06) | 1.6742 (05) | 1.7240 (05) |
| 301 | -2.2387 (05) | -3.3737 (05) | -4.3390 (04) |
| 310 | -4.4344 (05) | -2.6466 (05) | 8.4421 (05) |
| 131 | -1.1119 (07) | -1.9318 (07) | 1.0485 (07) |
| 140 | 7.1464 (06) | 5.2120 (06) | 2.5250 (06) |
| 212 | 1.7678 (06) | -3.7008 (06) | 1.8701 (06) |
| 221 | 8.3056 (06) | 5.5557 (06) | -1.1770 (07) |
| 230 | -7.8189 (06) | 2.3123 (06) | -3.3247 (06) |
| 302 | 7.9979 (05) | 7.3305 (05) | -7.3965 (05) |
| 311 | -6.1924 (06) | -3.5841 (06) | 2.7844 (06) |
| 320 | -7.7974 (06) | -3.5995 (06) | 1.6942 (06) |
| 401 | 1.3605 (06) | 1.8954 (06) | 2.2822 (05) |
| 410 | 5.4670 (06) | 2.6969 (06) | -2.6931 (06) |
| 141 | 1.9547 (08) | 1.5121 (08) | - |
| 150 | -3.4461 (07) | -2.2251 (07) | - |

| | | | |
|---|---|---|---|
| 222 | 1.4282 (08) | 1.0803 (08) | - |
| 231 | -1.4167 (08) | -7.5232 (07) | - |
| 240 | -1.5899 (07) | -1.8487 (07) | - |
| 303 | 1.3291 (07) | 1.3066 (07) | - |
| 312 | -3.9782 (07) | -2.0204 (07) | - |
| 321 | -7.7294 (06) | -8.8936 (06) | - |
| 330 | 7.1772 (07) | 1.6252 (07) | - |
| 402 | -6.9109 (06) | -7.6809 (06) | - |
| 411 | 3.4405 (07) | 1.4213 (07) | - |
| 420 | -2.8667 (06) | 6.7455 (06) | - |
| 501 | -2.6114 (06) | -2.4987 (06) | - |
| 510 | -1.6251 (07) | -8.5835 (06) | - |
| $\beta^{(3)}_{CO}$ | 1.92 (00) | 1.92 (00) | 1.89 |
| $\beta^{(3)}_{OO}$ | 1.98 (00) | 1.98 (00) | 2.36 |

Figures

Figure 1. Calculated potential energy curves of the ground singlet state of $CO_2$ ($^1$A'), and the three lowest triplet states, $^3$A', $1^3$A'', and $2^3$A'', at an OCO angle of $120^0$ and where one of the CO bond distances of 1.2 Å is fixed and the other is varied. The curves show these states at $C_s$ geometries to their O+CO dissociation limits, as a function of $r_{CO}$.

Figure 2a. Contour plot of the fitted potential for the $^3$A' state. Each panel is for a fixed OCO bond angle at $20^0$, $40^0$, $60^0$, $80^0$, $100^0$, $120^0$, $140^0$, $160^0$, $180^0$, starting at the left top panel. The two axes

are for each of the two $r_{CO}$ bond lengths in Å. Contour values are at -0.75 eV, -0.25 eV, 0.25 eV, 0.75 eV, 1.25 eV, 1.75 eV, 2.25 eV, 2.75 eV, 3.25 eV, and 3.75 eV.

Figure 2b. Same as Fig 1a. except for the $1^3A''$ state.

Figure 2c. Same as Fig 1a except for the $2^3A''$ state.

Figure 3a. Polar plot of the fitted potential for the $^3A'$ state. The carbon is at the origin and one of the oxygen atoms is fixed at -1.15 Å. The contours show the potential as a function of the position of the second oxygen atom. The axes are in Å. Contour values are at -0.75 eV, -0.25 eV, 0.25 eV, 0.75 eV, 1.25 eV, 1.75 eV, 2.25 eV, 2.75 eV, 3.25 eV, and 3.75 eV.

Figure 3b. Same as Fig 2a except for the $1^3A''$ state.

Figure 3c. Same as Fig 2a except for the $2^3A''$ state.

Figure 4. Vibrational relaxation rate for the process $O(^3P)+CO(^1\Sigma^+)(v=1\rightarrow v'=0)$ as a function of inverse temperature. — present results; ρ data of Center, Ref. 1; data of Lewittes *et al.*, Ref. 2: --- theoretical results of Kelley and Thommarson, Ref. 20.

Figure 5. Oxygen atom exchange rate for the process $^{18}O(^3P)+C^{16}O(^1\Sigma^+)\text{->}^{16}O+C^{18}O(^1\Sigma^+)$ as a function of inverse temperature. — present results; ◊ data of Garnett *et al.*, Ref. 6, O data of Jaffe and Klein, Ref. 7.

Figure 6. Vibrational excitation cross sections for the process $O(^3P)+CO(^1\Sigma^+)(v=0\rightarrow v')$ as a function of collision energy. — present results for the summed cross section $\sigma(0\rightarrow1)+2\sigma(0\rightarrow2)+3\sigma(0\rightarrow3)+\ldots$; --- present results for the cross section $\sigma(0\rightarrow1)$; O data of Upschulte and Caledonia, Ref. 11.

Figure 7a. Theoretical emission spectra from the nascent distribution of CO for the process $O(^3P)+CO(^1\Sigma^+)(v=0\rightarrow v')$ at 3.4 eV (8 km/s) collision energy at 5 $cm^{-1}$ resolution. Labels show locations of v' band heads of the excited CO.

Figure 7b. The same as 7a. — present results degraded to 70 $cm^{-1}$; --- , data of Upschulte and Caledonia, Ref. 11. Both results are normalized to be 1.0 at their maxima.

Figure 8. Theoretical cross sections for the process $O(^3P)+CO(^1\Sigma^+)(v=0\rightarrow v')$ at collision energies of 0.5 eV, 1.0 eV, 2.0 eV, 3.0 eV, and 4.0 eV.

Figure 9. Theoretical cross sections for the process $O(^3P)+CO(^1\Sigma^+)(v=0\rightarrow v')$ at a collision energy of 3 eV broken down into contributions from each final electronic state.

Figure 10. Ratios of reactive to non-reactive cross sections for the process $O(^3P)+CO(^1\Sigma^+)(v=0\rightarrow v'=1)$ for each final electronic state as a function of collision energy.

Figure 11. Slices of the fitted potential energy curves near the barrier region for the $^3A'$ state and $1^3A''$ states of $CO_2$. The OCO bond angle is fixed at $100^0$, and one of the $r_{CO}$ bond distances is fixed at the calculated equilibrium value of CO at 1.15 Å.

Figure 12a. Reactive (solid line) and nonreactive (dashed line) cross sections for the process $O(^3P)+CO(^1\Sigma^+)(v=0\rightarrow v')$ at a collision energy of 3 eV. Contribution from the $^3A'$ state.

Figure 12b. Same as Fig. 12a except for the $1^3A''$ state.

Figure 12c. Same as Fig. 12a except for the $2^3A''$ state.

Figure 13a. Theoretical rotational cross sections for the process $O(^3P)+CO(^1\Sigma^+)(v=0\rightarrow v'=0,1)$ at a collision energy of 3 eV.

Figure 13b. Surprisal plots of the rotational distributions shown in Fig. 13a. o v'=0, ρ v'=1.

Figure 14. Polar plot of the $^3A'$ potential energy surface as in Fig 3a with positions of the approaching $O(^3P)$ superimposed at point of closest approach for the process $O(^3P)+CO(^1\Sigma^+)(v=0\rightarrow v')$ at a collision energy of 3eV drawn from a random distribution of trajectories where v'>0: o, position of $O(^3P)$ when it is closest to the center of mass of the target CO for non-reactive collisions; x, position of $O(^3P)$ when the sum of bond lengths $r_{CO}+r_{OO}+r_{CO}$ are at a minimum for reactive collisions.

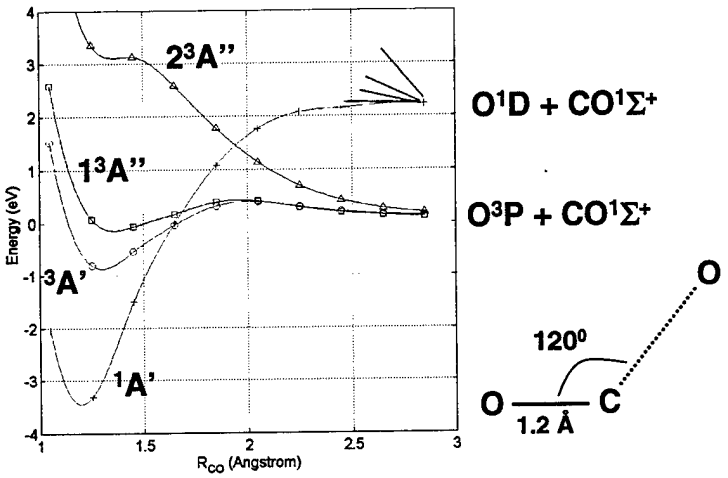


Figure 1

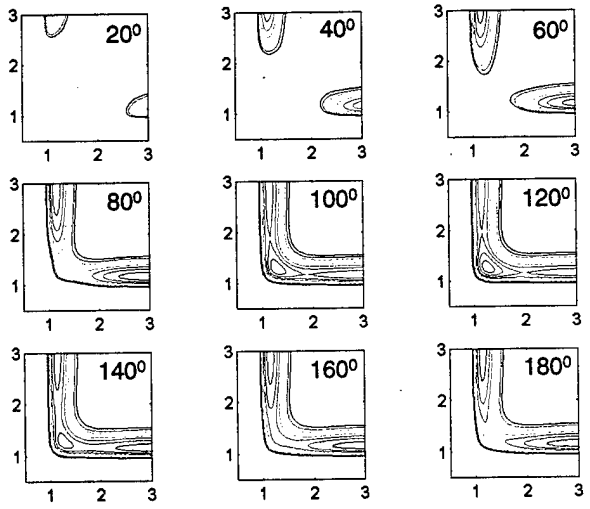


Figure 2a

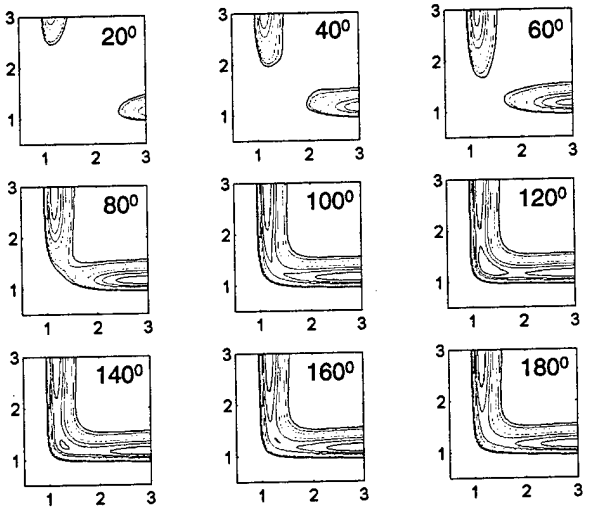


Figure 2b

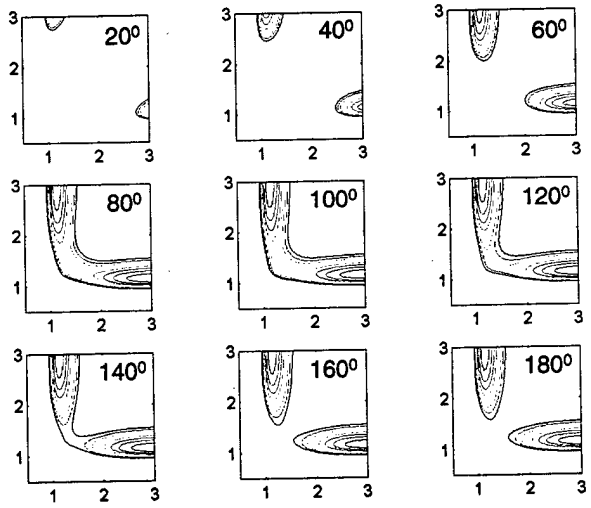


Figure 2c

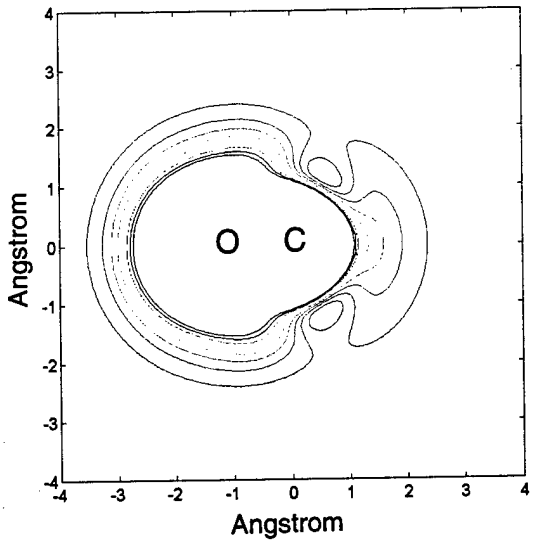


Figure 3a

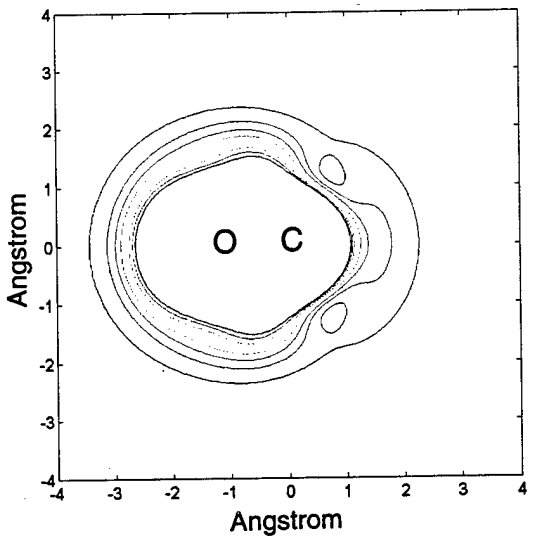


Figure 3b

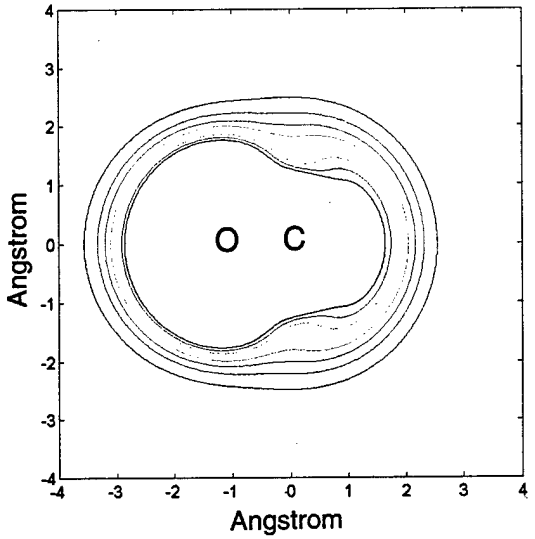


Figure 3c

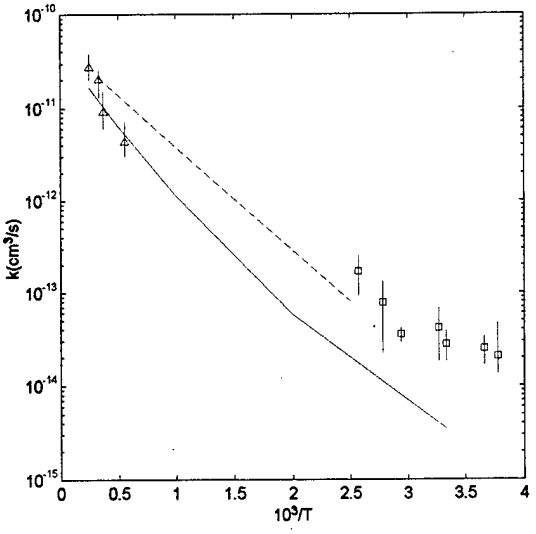


Figure 4

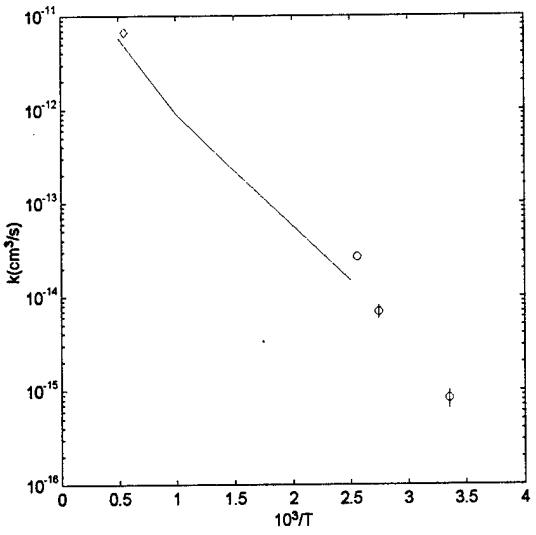


Figure 5

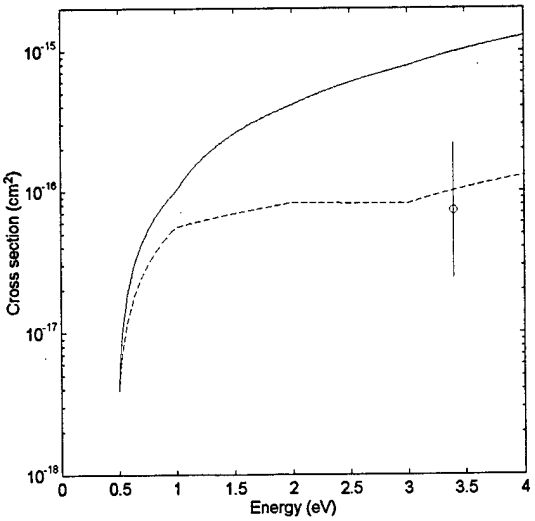


Figure 6

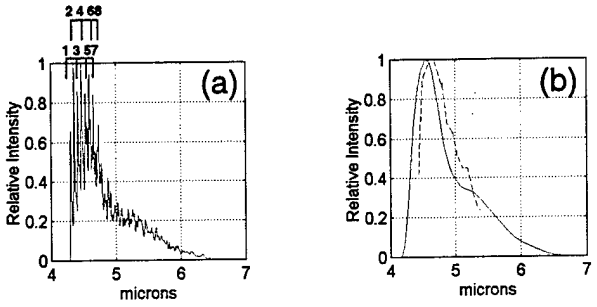


Figure 7

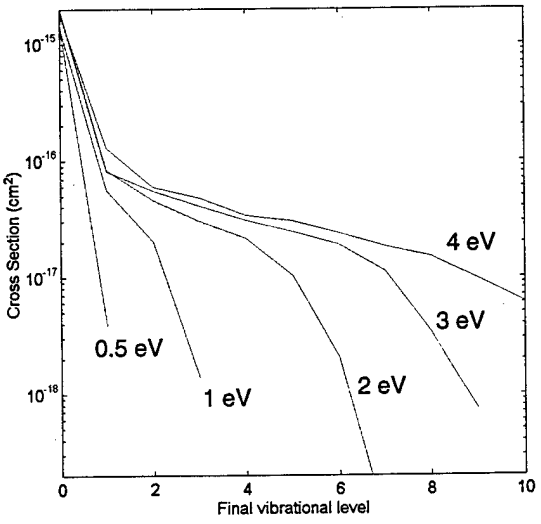


Figure 8

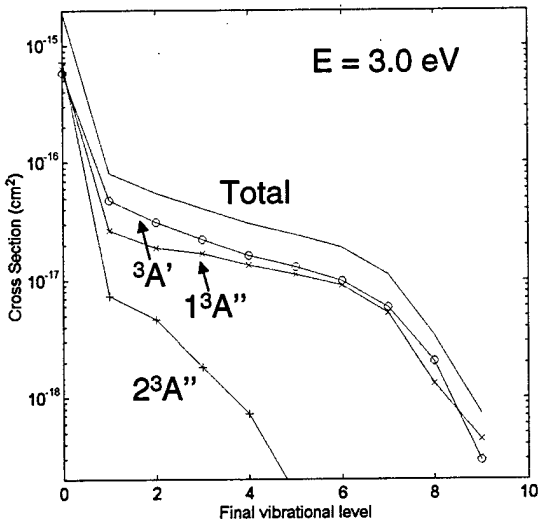


Figure 9

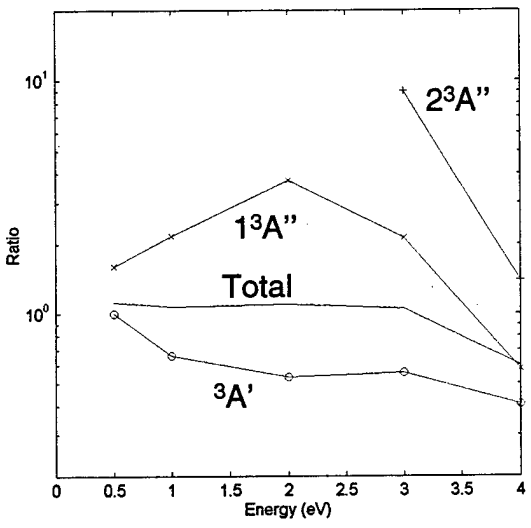


Figure 10

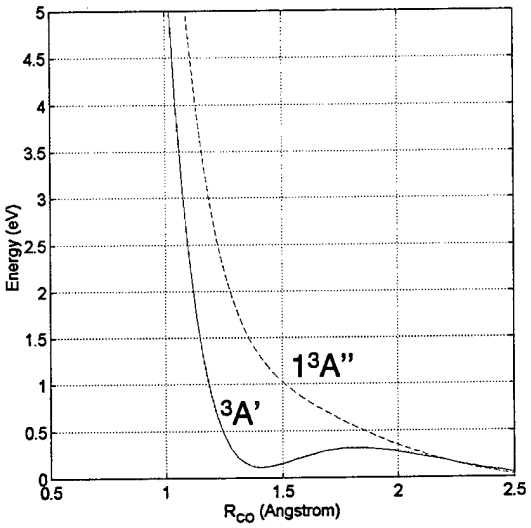


Figure 11

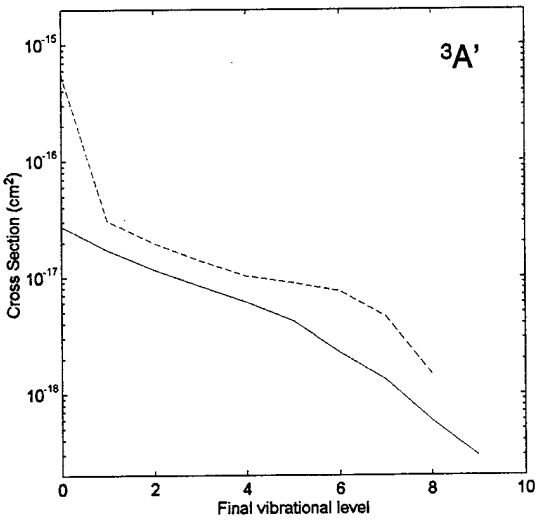


Figure 12a

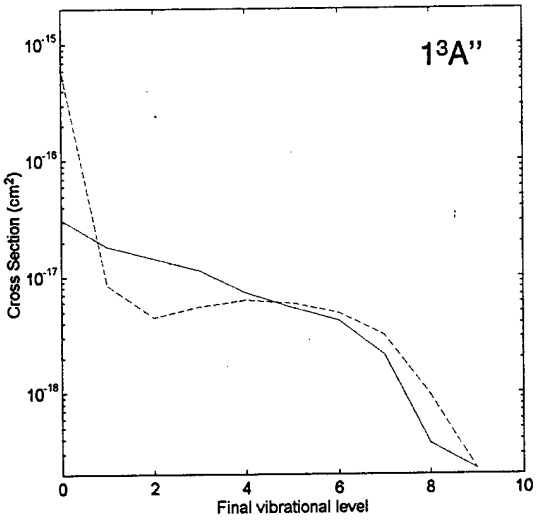


Figure 12b

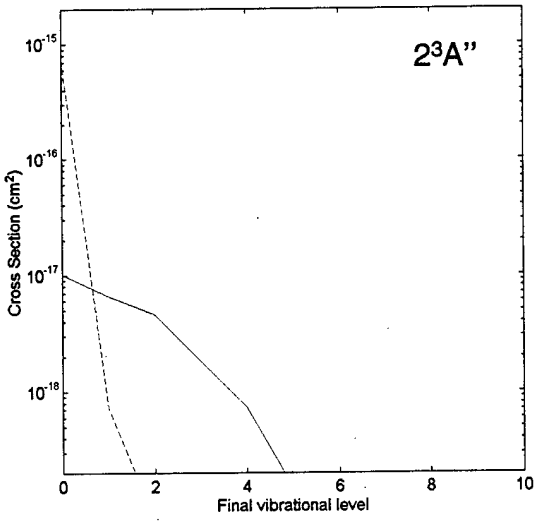


Figure 12c

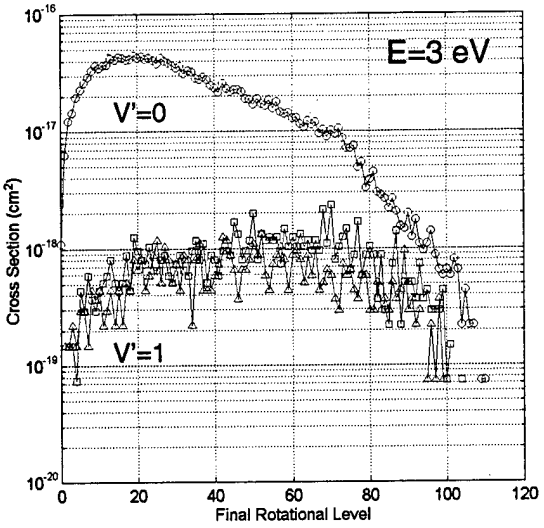


Figure 13a

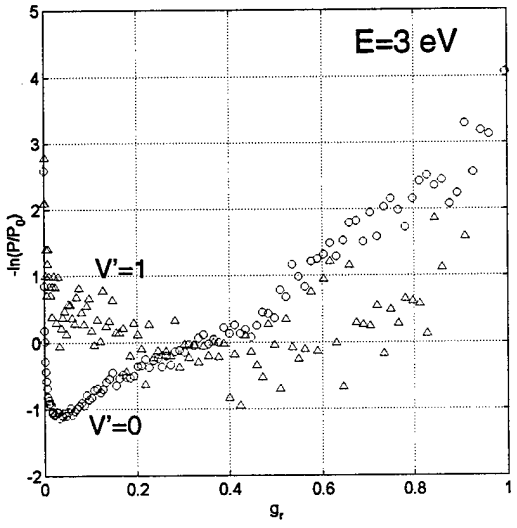


Figure 13b

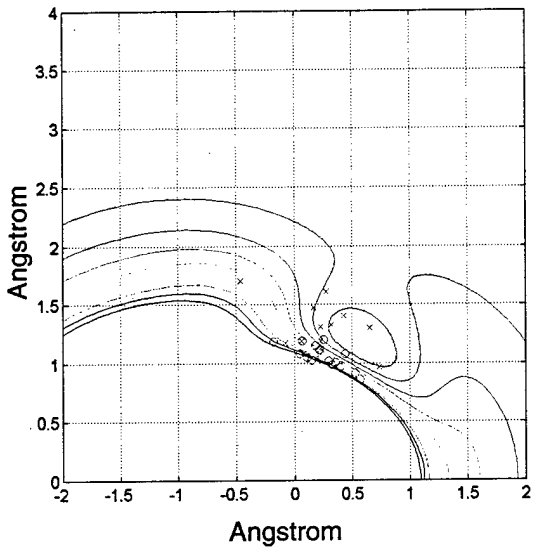


Figure 14